Supplement of Atmos. Meas. Tech., 19, 3445–3457, 2026
https://doi.org/10.5194/amt-19-3445-2026-supplement

Atmospheric Measurement Techniques
Open Access
EGU

Supplement of

Particle nitrate measurement using a thermal-dissociation, cavity-ringdown-spectrometer with gas-phase denuder (D-TD-CRDS)

Patrick Dewald et al.

Correspondence to: John N. Crowley (john.crowley@mpic.de)

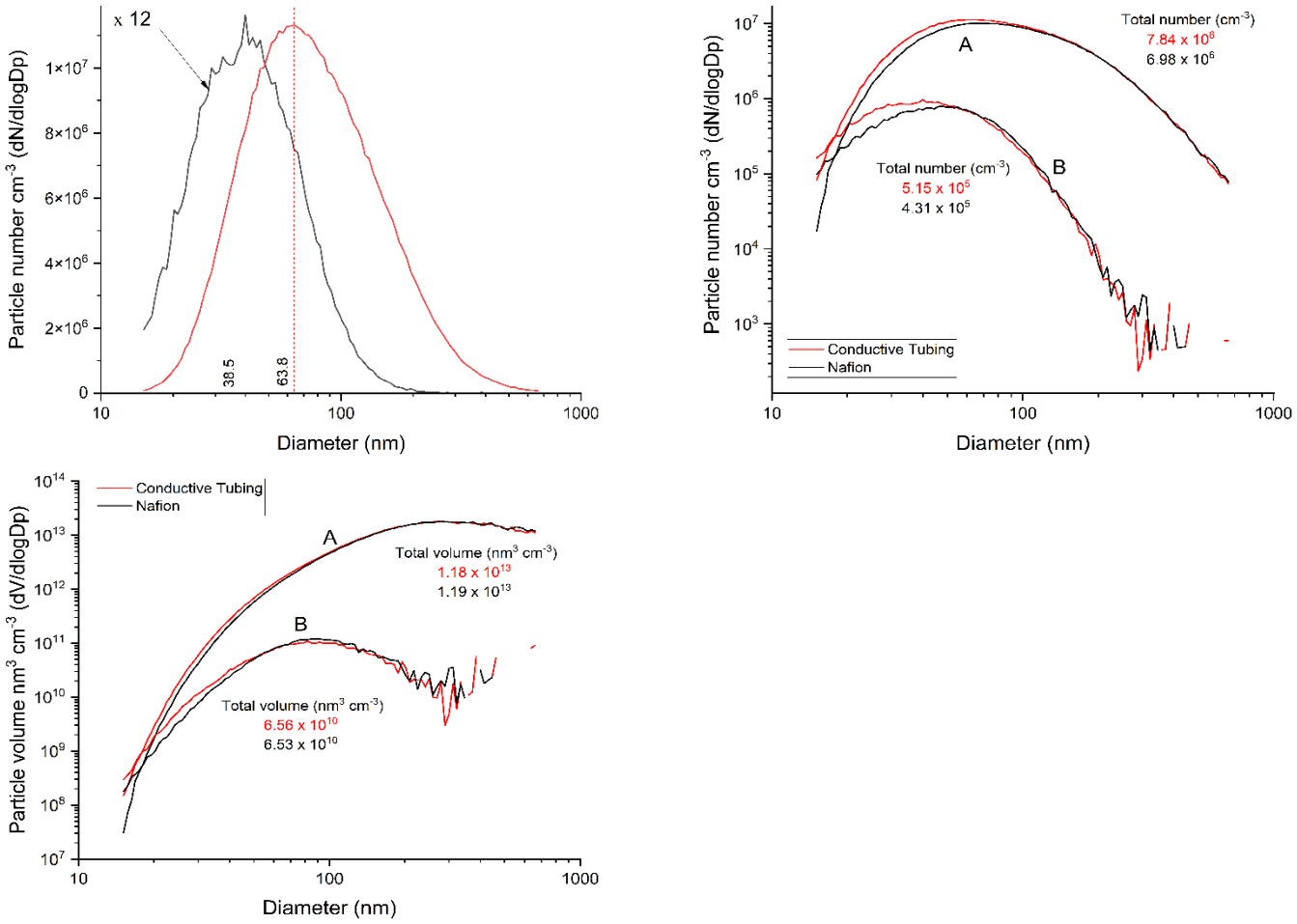

Figure S1 Top left: Ammonium sulphate particle distributions as used to test the particle transmission of the Nafion drier. The data obtained using the less concentrated ammonium sulphate solution (black line) has been scaled by a factor of 12. Top right and bottom: Particle size distributions through conductive tubing as reference (red lines) and the Nafion drier (black lines). The totals indicate the summed particle numbers and volume per cm^3 of air in each experiment. The data denoted "A" and "B" were obtained using the "concentrated" and "dilute" ammonium sulphate solutions, respectively.

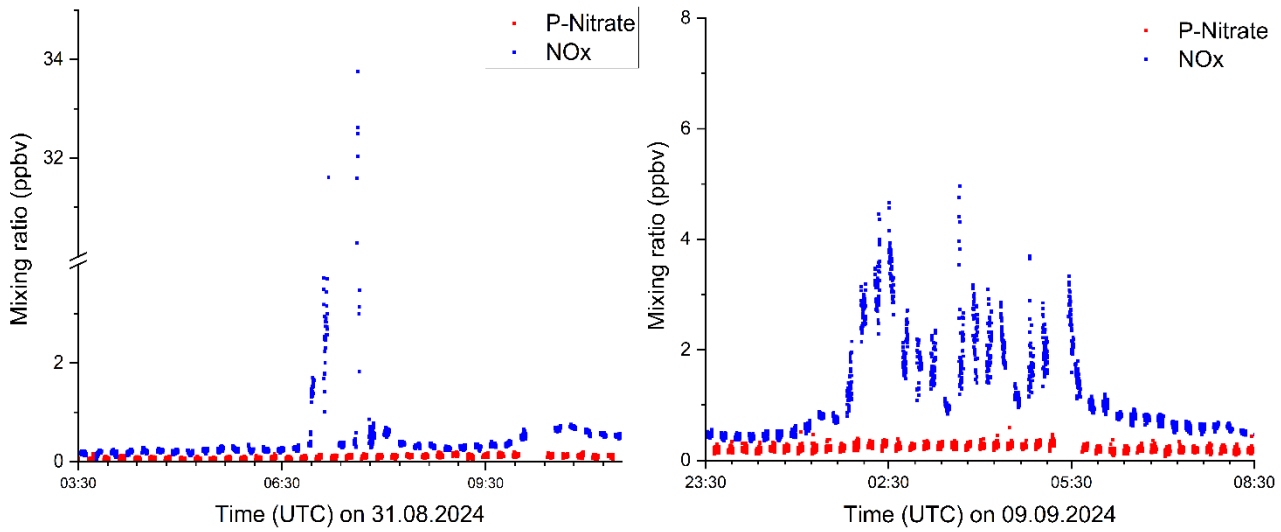

Figure S2 Examples demonstrating denuder efficiency during a campaign in the Boreal forest in 2024. No increase in signal is observed in the P-Nitrate channel (red) despite spikes of up to 34 ppbv of NO_X (31.08.2024) due to local vehicular emissions or prolonged exposure to several ppbv of NO_X (09.09.2024) as monitored by the NO_X channel (blue).

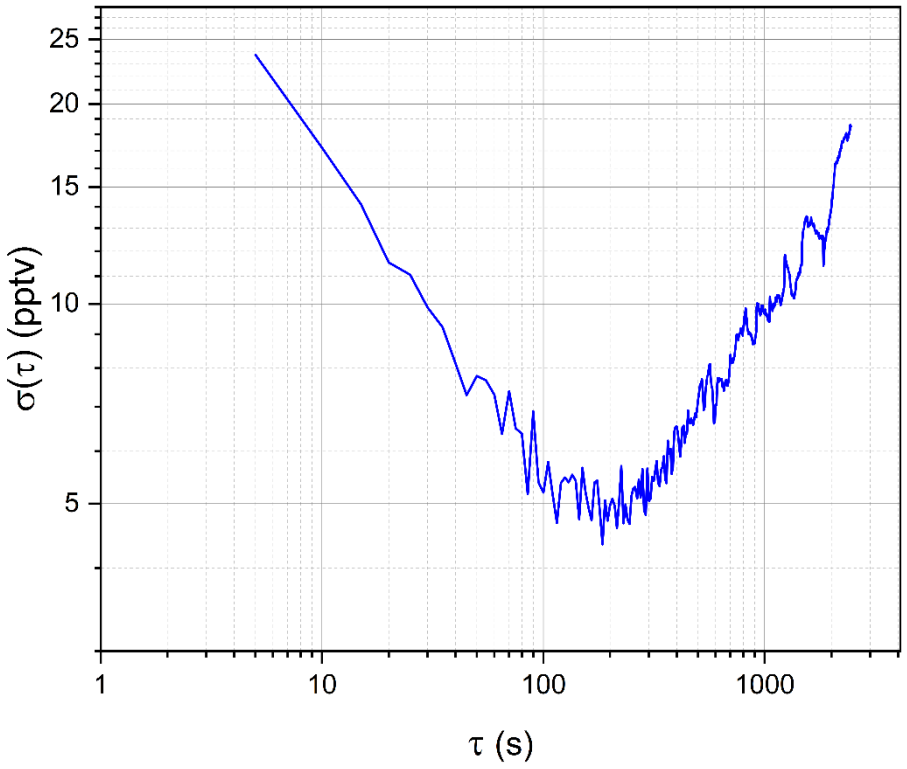

Figure S3. Allan deviation plot of data obtained when zeroing the P-Nit channel under laboratory conditions. Single ring down constants (k_0) were obtained by averaging for 5s at a laser modulation rate of 2400 Hz.

Calibration of the HR-ToF-AMS ionization efficiency

Inorganic nitrates (IP-Nit): Dry ammonium nitrate (NH_4NO_3) particles were generated using an atomizer (TSI, model 3076) and an aerosol diffusion drier (TSI model 3062) filled with silica gel as drying agent. The air exiting the diffusion drier was passed through a DMA (TSI, model 3082) to select a certain particle size. The resulting aerosol was simultaneously sampled by a CPC (TSI, model 3787) and the HR-ToF-AMS both sampling through similar lengths (< 50 cm) of conductive tubing. The ionization efficiency (IE) was derived from the ratio between the ions per second (I_{NO_3}) as detected by the AMS and the number of molecules per second (MPS) deduced from the SMPS measurement according to Eq. (1),

$$IE = \frac{I_{NO_3}}{MPS} = \frac{I_{NO_3} \cdot M_{NO_3}}{C_n \cdot Q \cdot N_A * \rho_p \cdot \frac{\pi}{6} \cdot d_{mob}^3 \cdot S \cdot f_{NO_3}} \quad \text{(S1)}$$

with the HR-ToF-MS signal I_{NO_3} on *m/z* 30 and *m/z* 46, the molecular weight M_{NO_3} of the nitrate ion (62 g mol^{-1}), the particle number concentration C_n from the CPC, the sampling flow rate Q of the AMS (1.2 cm^3 s^{-1}), the Avogadro constant N_A (6.022 x 10^{23} molecule mol^{-1}), the density ρ_p of ammonium nitrate (1.72 g cm^{-3}), the mobility diameter of the particle d_{mob}, the Jayne shape factor (S = 0.8 for dry ammonium nitrate) and the fraction of nitrate f_{NO_3} in the particles (0.775).

In our experiments, we selected particles with nominal mobility diameters of 101.4 nm, 153.4 nm or 350 nm. Figure S3 shows the correlation between I_{NO_3} and MPS together with an unweighted linear regression. A collection efficiency (CE) of 1 is assumed. Error propagation of the uncertainties associated with C_n (5% as stated by the manufacturer), S (6%, (Takegawa et al., 2005)) and d_{mob} (3% as stated by the manufacturer) results in an uncertainty of 12% associated with the MPS value. An uncertainty of 10% in I_{NO_3} is caused by fluctuations in voltages, the filament current, particle losses and counting statistics. The slope of the plot of I_{NO_3} versus MPS is IE = (7.41 ± 0.11) x 10^{-8} ion molecule^{-1} for ammonium nitrate. Error propagation from the uncertainties in MPS, I_{NO_3} and the linear regression (2%) yields an overall uncertainty of 16% for the ionization efficiency.

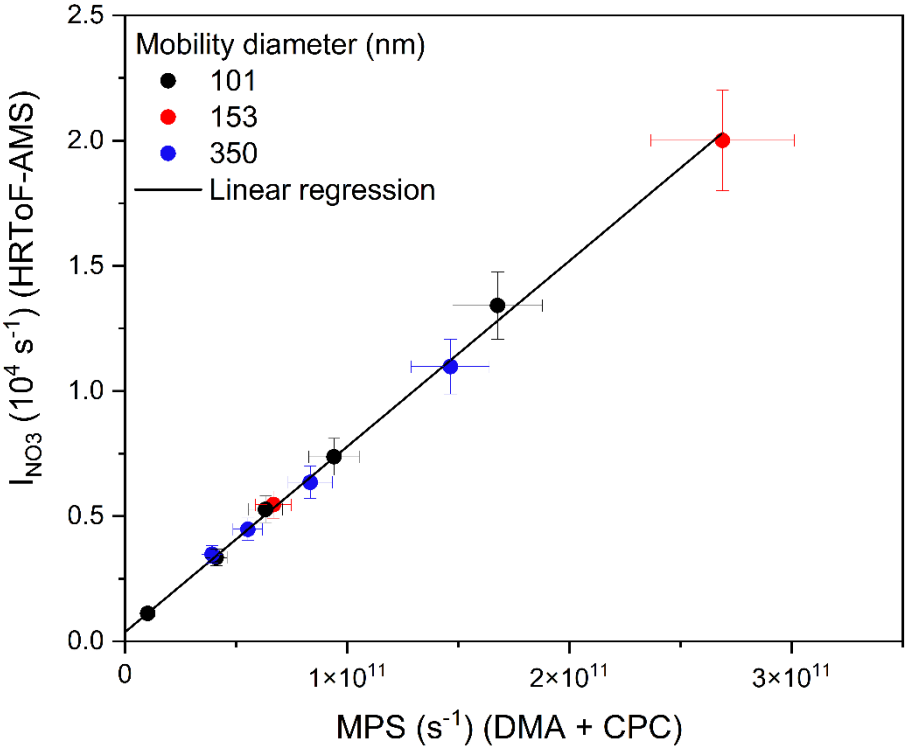

Figure S4: Summed HR-ToF-AMS signals ($\boldsymbol{I_{NO_3}}$) on *m/z* = 30 and *m/z* = 46 from ammonium nitrate particles (with mobility diameters of 101, 153 and 350 nm) plotted against the MPS. The error bars denote the associated uncertainties. An unweighted linear fit to the data yields a slope (IE) of (7.41 ± 0.11) x 10^{-8} ions molecule^{-1}, an intercept of (368 ± 128) ions s^{-1} and a Pearson correlation coefficient (r) of 0.999.

Organic Nitrates (OP-Nit): The HR-ToF-AMS was calibrated based on SMPS measurements of secondary organic aerosol (SOA) formed during an NO_3 + limonene oxidation experiment in the SCHARK atmospheric simulation chamber. The chamber was operated in dynamic mode with 25 SLPM dry synthetic air, resulting in an air exchange frequency of 4.55 x 10^{-4} s^{-1}. Apart from the HR-ToF-AMS and SMPS, a 5-channel-cavity-ringdown-spectrometer to measure NO_3, N_2O_5, and organic nitrates (Dewald et al., 2021; Sobanski et al., 2016) and the D-TD-CRDS sampled from the SCHARK at the same time and the non-denuded channels of the D-TD-CRDS were used to monitor NO_X and NO_Y. The data obtained are presented as a time series in Figure S5.

Between 09:20 and 09:36 UTC, a flow of limonene was introduced into the chamber which resulted in the complete loss of both NO_3 and N_2O_5, as expected. At 10:17 UTC, another 10 min flow of synthetic air (500 sccm) over the N_2O_5 crystals resulted in the reappearance of NO_3 and N_2O_5 as the limonene was consumed. This second addition of N_2O_5 resulted in the formation of ~5 ppbv of gas-phase organic nitrates and 2.8 ppbv of OP-Nit at 10:35 UTC.

Note that the denuder channel (labelled OP-Nit) does not detect the several ppbv of NO_Z present in the SCHARK between ~ 08:30 and 09:20 UTC.

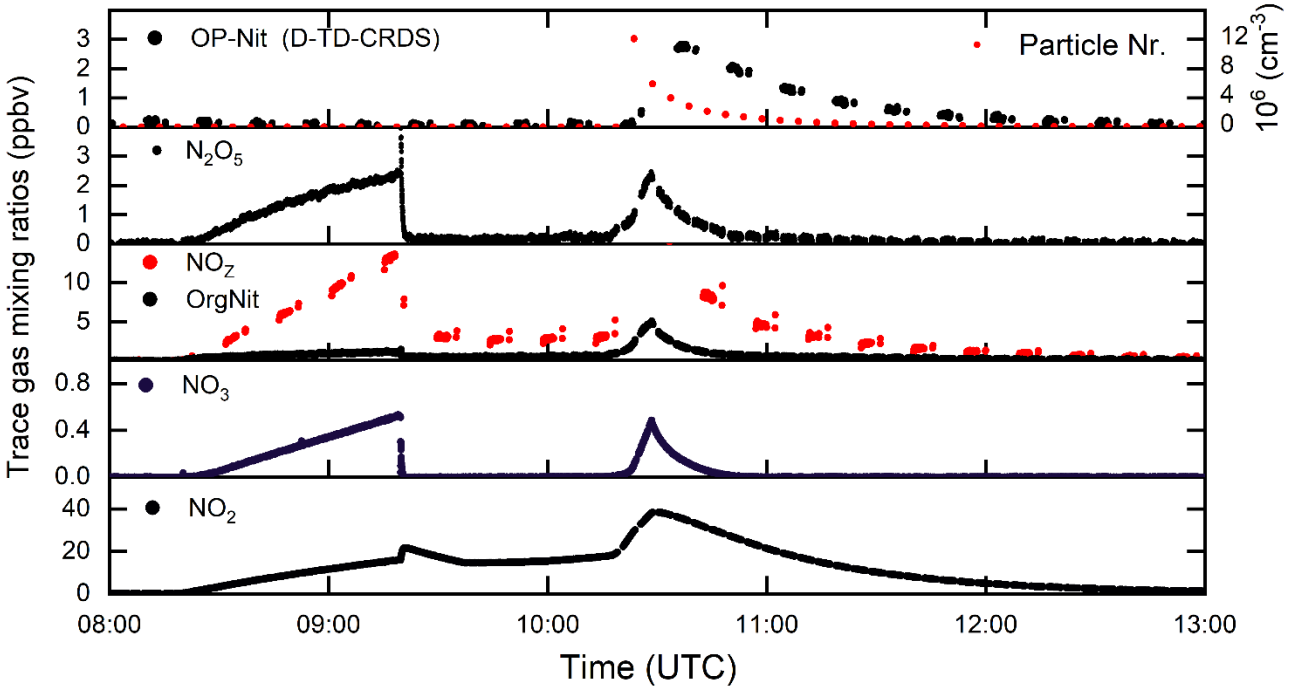

Figure S5: Detection of relevant trace gases and particulate matter during a SCHARK experiment dedicated to generate OP-Nit via the NO_3-initiated oxidation of limonene.

The SMPS measured a peak in the particle number concentration at 10:28 UTC (upper panel) shortly after the second N_2O_5 addition following which the number concentration decreased continuously. At the same time, the mobility diameter of the particles increased as the particles coagulated. Apart from at the onset of particle formation, when the volume weighted mode maximum diameter (d(v)) was < 50 nm, the particles were characterised by d(v) > 60 nm.

The average HR-AMS mass spectrum at 10:30 UTC (Fig. S6) from this period shows that the majority of the nitrate moiety is detected at *m/z* 30 with ca. 11% at *m/z* 46. In this calibration ca. 17 % of the signal at *m/z* 30 was caused by organic fragments; the nitrate aerosol mass was corrected via HR analysis in PIKA accordingly.

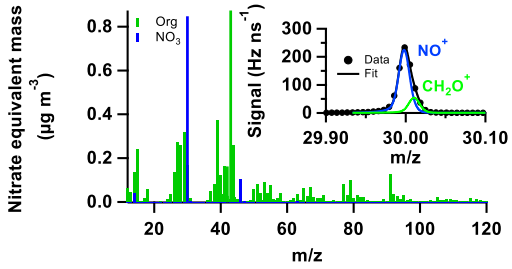

Figure S6. Average mass spectrum as derived from the AMS during this experiment coloured by species. The inset shows details of the signal (Diff.) at *m*/*z* 30, which is the dominant fragment for the quantification of organic nitrates.

For particles with $d(v) > 60$ nm, the number of molecules per second (MPS) was calculated as in Eq. (S1) by directly using the particle volume concentration in $nm^3\ cm^{-3}$ provided by the SMPS and the flow rate of the AMS. Furthermore, we adopted the SOA properties resulting from the NO_3 + limonene oxidation reported in DeVault et al. (2022), i.e. a density of 1.18 g cm^{-3} (7% uncertainty), a molecular weight of 210 g mol^{-1} (1% uncertainty), and we assumed that each SOA molecule formed contains one nitrate functional group (30% uncertainty). The last assumption not only results in an f_{NO_3} in the particles of 0.295, but also increases the uncertainty in MPS to 32%. A "Jayne shape factor" of $S = 1.21$ (9% uncertainty) was estimated by comparing the vacuum aerodynamic diameter from the PToF data (AMS) with the mobility diameter from the DMA as described in DeCarlo et al. (2006). The ion-signal is plotted against the calculated MPS (Fig. S7). An unweighted linear regression indicates a detection efficiency (CE x IE) of 6.64 x 10^{-8} ions $molecule^{-1}$ with a total uncertainty of 34%. Figure S7 also shows that particles with $d(v) < 60$ nm are not detected as efficiently, which is related to their lower transmission through the aerodynamic lens (Liu et al., 2007). The fact that we see no significant deviation in the slope from particles with $d(v)$ between 57 and 71 nm indicates that our calibration is applicable for larger particles also.

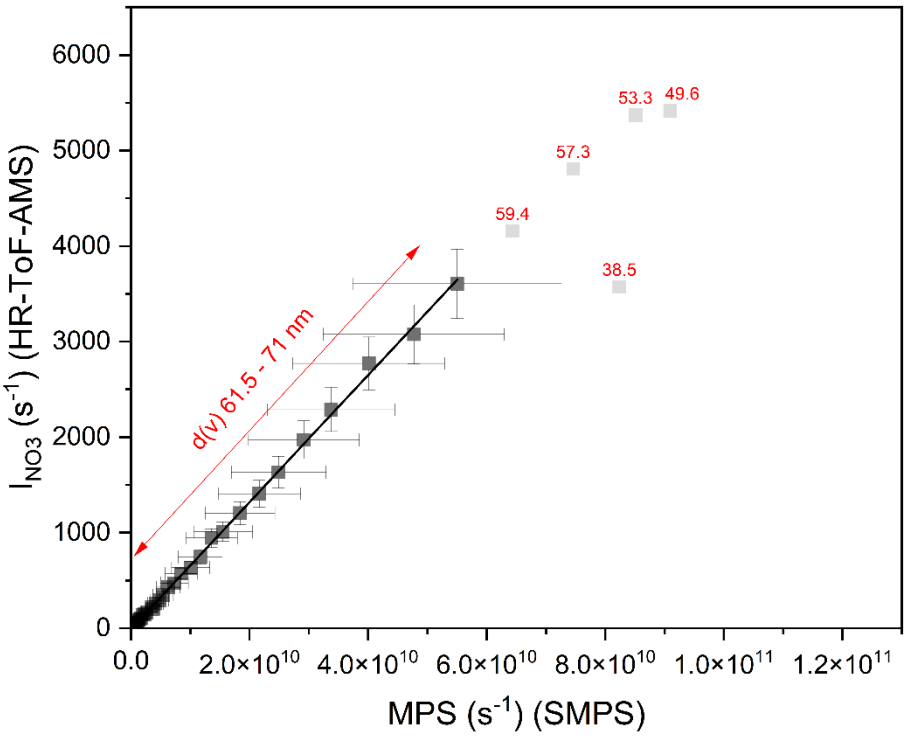

Figure S7: Summed HR-ToF-AMS signals (black datapoints) on *m*/*z* 30 and *m*/*z* 46 induced by OP-Nit plotted against the MPS as calculated from the SMPS data according to Eq. (S1). The error bars denote the associated uncertainties. An unweighted linear fit to the data yields a slope (IE x CE) of (6.64 ± 0.04) x 10^{-8} ion $molecule^{-1}$, an intercept of (-5.5 ± 8.0) ion s^{-1} and a Pearson correlation coefficient (r) of 0.9994.

References

DeCarlo, P. F., et al.: Field-Deployable, High-Resolution, Time-of-Flight Aerosol Mass Spectrometer, Anal. Chem., 78, 8281-8289, 2006.

DeVault, M. P., et al.: Products and Mechanisms of Secondary Organic Aerosol Formation from the NO3 Radical-Initiated Oxidation of Cyclic and Acyclic Monoterpenes, ACS Earth and Space Chemistry, 6, 2076-2092, 2022.

Dewald, P., et al.: Impact of ozone and inlet design on the quantification of isoprene-derived organic nitrates by thermal dissociation cavity ring-down spectroscopy (TD-CRDS), Atmos. Meas. Tech., 14, 5501-5519, 2021.

Liu, P. S. K., et al.: Transmission efficiency of an aerodynamic focusing lens system: Comparison of model calculations and laboratory measurements for the Aerodyne Aerosol Mass Spectrometer, Aerosol Science and Technology, 41, 721-733, 2007.

Sobanski, N., et al.: A five-channel cavity ring-down spectrometer for the detection of NO_2, NO_3, N_2O_5, total peroxy nitrates and total alkyl nitrates, Atmos. Meas. Tech., 9, 5103-5118, 2016.

Takegawa, N., et al.: Characterization of an Aerodyne Aerosol Mass Spectrometer (AMS): Intercomparison with other aerosol instruments, Aerosol Science and Technology, 39, 760-770, 2005.